J. Chem. Sci. Vol. 127, No. 11, November 2015, pp. 2005–2014.
DOI 10.1007/s12039-015-0971-2

Copper inorganic-organic hybrid coordination compound as a novel L-cysteine electrochemical sensor: Synthesis, characterization, spectroscopy and crystal structure

ZOHREH DERIKVAND* and AZADEH AZADBAKHT

Department of Chemistry, Faculty of Science, Khorramabad Branch, Islamic Azad University, Khorramabad, Iran
e-mail: zderik@yahoo.com

MS received 24 May 2015; revised 27 August 2015; accepted 1 September 2015

Abstract. Dinuclear coordination compound of Cu(II), namely, $[Cu_2(pydc)_2(pz)(H_2O)_2]\cdot 2H_2O$, where pydc = pyridine-2,6-dicarboxylic acid (dipicolinic acid) and pz = pyrazine has been synthesized and characterized by elemental analysis, spectra (IR, UV-Vis), thermal (TG/DTG) analysis, magnetic measurements and single crystal X-ray diffraction. In the dimeric structure, the planar tridentate pyridine-2,6-dicarboxylic acid dianion coordinates to a Cu(II) ion in a meridional fashion and defines the basal plane of the complex. The fourth equatorial coordination site is then occupied by a pyrazine molecule that functions as a linear bidentate ligand bridging two Cu(II) complexes to form a dimer. The axial positions of each Cu(II) complex are occupied by one water molecule to form a distorted square pyramidal geometry. The complicated hydrogen bonding network accompanied with C–O$\cdots\pi$ and C–H$\cdots\pi$ stacking interactions assemble the crystal structure of **1** into a fascinating supramolecular architecture. Electrochemical behavior of $[Cu_2(pydc)_2(pz)(H_2O)_2]$ (Cu-PDAP) on the surface of carbon nanotube (CNTs) glassy carbon electrode (GCE) is described. Oxidation of cysteine on the surface of modified electrode was investigated with cyclic voltammetry and electrochemical impedance spectroscopy (EIS). The results show that the Cu-PDAP/CNTs film displays excellent electrochemical catalytic activities towards L-cysteine oxidation.

Keywords. Pyridine-2,6-dicarboxylic acid; Crystal structure; Dinuclear complex; Electrocatalysis; Impedance spectroscopy.

1. Introduction

The design and construction of inorganic–organic hybrid materials attract great attention in the fields of crystal engineering and supramolecular chemistry, owing to fascinating topological architectures and powerful potential applications in various areas, such as nonlinear optics, magnetism, heterogeneous catalysis, gas storage and luminescent materials.[1–11] Predicting the final structures of demanded crystalline products is a great challenge. The self-assembly process of crystalline products is influenced by various factors, such as metal salt, organic ligands, counter ions, solvent system, temperature and pH of the reaction system.[12–14] The reports demonstrate that the π-conjugated N-donor bridging ligands such as pyrazine and aromatic dicarboxylic acids acting as organic ligands have been extensively utilized in the preparation of coordination compounds.[15–19]

Supramolecular architectures based on non-covalent interactions such as aromatic–aromatic stacking, donor–acceptor interactions and hydrogen bonding, are interesting and have attracted an enormous attention. In recent years, considerable effort has been made to understand the relationship between the molecular geometry and the crystal structure in terms of the prevalent hydrogen-bonding patterns.[20] The various strong and weak hydrogen bonds have the powerful directional effect to organize individual molecules into supramolecular architectures as ribbons, rosettes, layers, tubes, rods, spheres and sheets.[21] The electrochemical reactions catalyzed by transition metal complexes have also received significant attention during the past decades.[22]

Transition metal elements of ruthenium, iron, platinum, iridium, manganese, cobalt, tungsten, zinc and vanadium in different forms such as metals or metal oxide, metallocyanides and organometallic complexes have been successfully dispersed on some substrates such as carbon on conductive polymers to make catalysts. The immobilization of transition metal compound

*For correspondence

onto carbon nanotubes increased the catalytic activity of the modified surfaces.[23–26] Due to this fact, we constructed a novel functional hybrid film of carbon nanotube and $[Cu_2(pydc)_2(pz)(H_2O)_2]$ (Cu-PDAP) on a glassy carbon electrode as a catalytic layer for L-cysteine detection. Results show that Cu-PDAP exhibits a remarkable electrocatalytic activity for oxidation of L-cysteine. The proposed sensor possesses high sensitivity and stability and so it has the promising future for practical application.

2. Experimental

2.1 *General methods and materials*

All materials were purchased from Merck. Solvents used throughout the reactions were of high purity. Multiwall carbon nanotubes with purity 95% (10–20 nm diameters) and 1 μm length were obtained from Nanolab (Brighton, MA). IR spectroscopy was performed on a Perkin-Elmer Spectrum RXI FT-IR spectrophotometer in the 4000-400 cm^{-1} region using a KBr pellet. The UV-Vis spectra were recorded on a JELWAY 6505 UV-Vis spectrophotometer and a Shimadzu 2100 spectrophotometer in the range of 200–900 nm at room temperature. Elemental analysis was performed with a Heraus CHN Pro apparatus. The X-ray data were obtained with a Bruker SMART ApexII diffractometer. Thermal analyses (TG–DTG–DTA) including the thermogravimetery (TG), derivative thermogravimetery (DTG) and differential thermal analysis (DTA) were carried out using a Perkin Elmer simultaneous thermal analyzer (STA Pyris Diamond Model) with the heating rate of 10°C/min in N_2 atmosphere. Electrochemical experiments were performed via using a μAutolab III (Eco Chemie B.V.) potentiostat/galvanostat by NOVA 1.8 software. A conventional three electrode cell was used with an Ag|AgCl electrode (KCl 3 M) as the reference electrode, a Pt wire as counter electrode and a modified glassy carbon electrode (GCE) as working electrode. The cell was a one compartment cell with an internal volume of 10 mL. JENWAY pH meter (model 3345) was used for pH measurements.

2.2 *Crystal structure determination and refinement*

Suitable crystals of the synthesized compound were selected for X-ray data collection. Unit cell determinations and data collections were carried out using a Bruker SMART Apex II CCD area detector system[27] with Mo Kα radiation (λ = 0.71073 Å). The structure was solved and refined by full-matrix least-squares techniques on F^2 using the programs SHELXS and SHELXL, respectively.[28] Multi-scan absorption corrections were applied.

2.3 *Synthesis of $[Cu_2(pydc)_2(pz)(H_2O)_2]\cdot 2H_2O$ (**1**)*

An aqueous solution of $Cu(NO_3)_2\cdot 4H_2O$ (68 mg; 0.26 mmol) in water (5 mL) was added dropwise to a mixed ligand solution of pyridine-2,6-dicarboxylic acid (100 mg; 0.59 mmol) and pyrazine (47 mg; 0.59 mmol) in water (20 mL) under stirring in a 1:2:2 molar ratio, shown in scheme 1. The solution was heated very slightly (60°C) for 1 h, then was placed into Teflon line a stainless steel autoclave and heated to 140°C for 3 days and slowly cooled to room temperature at a cooling rate of 3°C per minute. Small needles blue crystals of the complex were collected in 73% yield. Anal. Calc. for $C_{18}H_{18}Cu_2N_4O_{12}$: C, 35.47; H, 2.98; N, 9.19%. Found: C, 35.24; H, 2.92; N, 9.06%. IR (KBr disc, υ/cm^{-1}): 3403 (b), 3384(b), 3084(b), 1638(s), 1594(s), 1436 (s), 1400(s), 1372(s), 1122 (s), 1040(s), 891(s), 846(s), 762(s), 682(s), 593(s), 554(w), 445(s).

2.4 *Electrode modification*

To prepare a modified electrode, GCE was polished with emery paper followed by alumina (1.0 and 0.05 μm) and then thoroughly washed with twice distilled water. This electrode was afterwards placed in ethanol container and then an ultrasonic cleaning bath was used to remove the adsorbed particles. Then, 25 μL solution of DMSO–CNTs (0.4 mg mL^{-1}) was cast on the surface of GC electrode and dried in air to form a CNTs film at electrode surface. Afterwards, the electrode was thoroughly rinsed with water and

Scheme 1. Synthesis route of preparation $[Cu_2(pydc)_2(pz)\ (H_2O)_2]\cdot 2H_2O$.

kept at room temperature for further use. The prepared CNTs/GC electrode was placed in DMSO solution with 0.1 M tetrabuthyl ammonium perchlorate as the supporting electrolyte containing 1×10^{-2} M Cu-PDAP and the electrode potential was cycled between −0.5 and 0.7 V at a scan rate of 50 mV s^{-1} for 100 cycles. The modified electrode (denoted as Cu-PDAP/CNTs/GCE) was thoroughly rinsed and cycled between −0.5 and 0.7 V in 0.1 M acetate buffer solution until a reproducible cyclic voltammogram (CV) was obtained.

3. Results and Discussion

3.1 *Synthesis and spectroscopic studies*

Treatment of $Cu(NO_3)_2$ with dipicolinic acid and pyrazine in 1:2:2 molar ratio under hydrothermal conditions gave compound **1** (scheme 1). The crystals were obtained by gradual cooling from 140°C to room temperature at a cooling rate of 3°C per minute. The obtained needles of blue crystals of compound **1** are stable in air and soluble in water, DMSO, DMF and MeOH. Elemental analysis of the complex is entirely consistent with its determined composition by X-ray crystallography.

The IR spectrum of **1** exhibits the characteristic stretching bands of carboxylate groups between 1372 and 1638 cm^{-1}. No strong absorption bands around 1700 cm^{-1} for –COOH are observed, demonstrating that carboxyl groups of organic moieties in **1** are completely deprotonated. The IR spectrum of compound **1** shows a broad band around 3403-3384 cm^{-1} due to υ(OH) stretching vibrations of water molecules. The band appears at around 1638 cm^{-1} due to the asymmetric stretching (υ_{as}) of the carboxylate group; the symmetrical stretching (υ_s) band of this group appears at 1372 cm^{-1}. The value of $\Delta[\upsilon_{as}-\upsilon_s]$ is 266 cm^{-1}, comparatively larger than 200 cm^{-1}, indicating monochelation of the carboxylic group to the metal ion,[29] which is in agreement with the X-ray crystal analysis.

The strong absorption bands at 1594 and 1435 cm^{-1} are attributed to the υ(C=C) and υ(C=N) vibrations in the ligands, respectively.[30] The υ(C–O) vibrations were observed at 1040 and 1272 cm^{-1}, as indicated in literature.[31–33] The ring wagging vibrations of the pyridine groups are also observed at 682 and 750 cm^{-1}. The weak bands at 592 and 450 cm^{-1} are from the Cu–N and Cu–O vibrations, respectively, for complex **1** (figure S1 in Supplementary Information).

The electronic spectrum of **1** was recorded in solid state with KBr and in solution at room temperature (figure 1). The electronic spectrum reveals absorption bands below 320 nm with high molar extinction coefficients that can be assigned to $\pi \rightarrow \pi^*$ and n $\rightarrow$ π^* intra-ligand transitions. In the solid state absorption spectra of the complex, there are similar absorption peaks due to the π–π^* and n $\rightarrow$ π^* transitions of ligands. The absorption band profiles in solution are similar to those absorption maxima of the complex **1** in the solid state. All the π–π^* and n $\rightarrow$ π^* transition bands for the copper (II) complex in water, DMF, MeOH and DMSO are observed in the range 220–320 nm. In the visible range, one broad peak was observed which can be assigned to $a_1 \rightarrow b_1$ transition.[34,35] The d–d transitions show a similar pattern with the peak maximum at 780 nm in the solid state, 773 nm in water, 768 nm in DMF, 771 nm MeOH, and 781 nm in DMSO and suggest that the Cu(II) ion has the characteristics of a penta-coordinated copper complex with distortion (figure 1).[36] All the data obtained from the electronic spectra in solutions do not show any noticeable differences from that of the solid state, so it may be assumed that the bonding modes of the ligands as well as the geometry of the complex do not change in solution state.[37] The room temperature magnetic moment of the Cu(II) complex is 1.65 BM per each Cu(II) ion in the crystal structure, demonstrating the presence of one unpaired electron in each cu(II) complex.

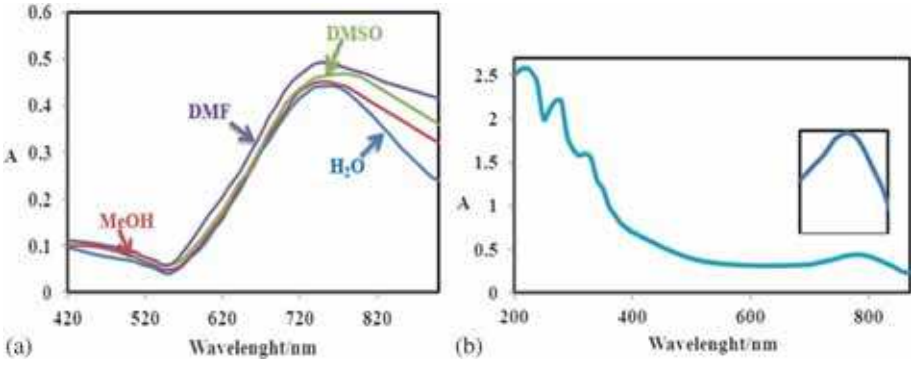

Figure 1. UV–Vis spectra of complex **1** (2.43×10^{-3} M) in solution (**a**), and (**b**) solid states.

3.2 *Crystal structure of $[Cu_2(pydc)_2(pz)(H_2O)_2]\cdot 2H_2O$ (**1**)*

The crystallographic data of **1** are summarized in table 1, selected bond lengths and angles as well as selected intermolecular hydrogen bond parameters are listed in tables 2 and 3, respectively. As shown in figure 2, compound **1** is a neutral dimeric structure consisting of two Cu(II) atoms, two $(pydc)^{2-}$ ligands, one pyrazine ligand, two coordinated and two uncoordinated water molecules. We provide here a more detailed analysis of the solid-state packing and used it for preparation a modified electrode for electrochemical catalytic activities towards L-cysteine oxidation. As shown in figure 2, the tridentate $(pydc)^{2-}$ ligand coordinates to Cu(II) uon in a meridional fashion and blocking three coordination sites of the square pyramid and the other two remaining sites were occupied by pyrazine as bridging ligand and one water molecule. Two such Cu(II) complexes are bridged by a pyrazine (μ_2) molecule through the equatorial coordination sites to form a dimer. The geometry of 5-coordinated compounds can be described either as a square pyramid or a trigonal bipyramidal with structural parameter $\tau(\tau = (\beta - \alpha)/60°)$, where β and α are the largest angles in the coordination sphere,[38] and its value is zero for a perfect square pyramid and one for a perfect trigonal bipyramid. The largest angles in **1**, N1-Cu1-N2 and O1-Cu1-O3 are 168.16 (5)° and 161.63 (4)° and resulting in $\tau = 0.11$. Therefore, the geometry can be described as distorted square pyramidal. The polyhedron geometry of diaqua-bis(pyridine-2,6-dicarboxylato-*O*, *N*, *O′*)-(μ_2-pyrazino)copper(II) dihydrate is illustrated in figure 2.

Two planes of 2,6-pyridinedicarboxylate ligands in the dimeric complex are parallel and form an

Table 1. Crystallographic data for compound **1**.

Crystal data	**1**
Empirical formula	$C_{18}H_{14}Cu_2N_4O_{10}\cdot 2(H_2O)$
Formula weight	609.44
Crystal system	Monoclinic
Space group	$P2_1/n$
a, Å	5.7535 (5)
b, Å	15.3205 (12)
c, Å	11.9486 (9)
β,°	92.524 (2)°
Z	2
V, Å^3	1052.21 (15)
Dcalc/(Mg.m^{-3})	1.924
$F(000)$	616
Refl. collected	2610
No. unique refl	2346, $R_{int} = 0.024$
Goodness-of-fit on F^2	1.014
R_1 $[I > 2\sigma(I)]$	0.022
wR_2 (all data)	0.063

Table 2. Selected bond distances (Å) and bond angles (°) for $[Cu_2(pydc)_2(pz)(H_2O)_2]\cdot 2H_2O$.

	Bond lengths		
Cu1−N1	1.8990(12)	Cu1−O1	2.0102(11)
Cu1−N2	1.9656(12)	Cu1−O3	2.0297(11)
Cu1−O5	2.1988(12)		
	Bond angles		
N1−Cu1−N2	168.16(5)	O1−Cu1−O3	161.63(4)
N1−Cu1−O1	81.45(5(	N1−Cu1−O5	94.63(5)
N2−Cu1−O1	96.26(5(	N2−Cu1−O5	97.10(5)
N1−Cu1−O3	80.64(5(	O1−Cu1−O5	93.31(5)
N2−Cu1−O3	100.45(5)	O3−Cu1−O5	92.15(5)

Table 3. Selected hydrogen bond geometry for compound **1**.

D–H···A	(D–H)Å	(H···A) Å	d(D···A) Å	(D–H···A)(°)
O5—H5A···O4^{i}	0.80 (3)	1.96 (3)	2.7534 (16)	168
O5—H5B···O6^{ii}	0.79 (3)	1.94 (3)	2.7260 (18)	174
O6—H6A···O2^{iii}	0.76 (3)	2.04 (3)	2.7956 (17)	171
O6—H6B···O4	0.82 (3)	2.05 (3)	2.8681 (17)	177
C3—H3···O2^{iv}	0.88 (2)	2.39 (2)	3.123 (2)	148
C5—H5···O5^{v}	0.93 (2)	2.54 (2)	3.574 (2)	149

Symmetry codes: (i) x-1/2, -y+1/2, z+1/2; (ii) x-1, y, z; (iii) -x+1/2, y-1/2, -z+1/2; (iv) -x-1, -y+1, -z; (v) x-1/2, -y-1/2, z-3/2.

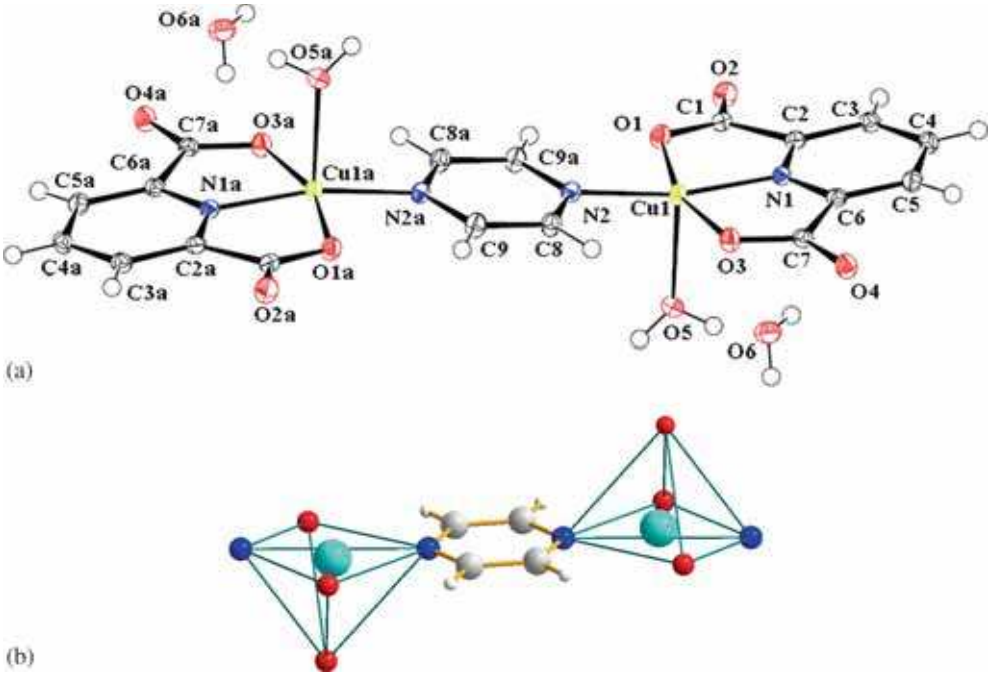

Figure 2. (**a**) Dimer structure of $[Cu_2(pydc)_2(pz)\ (H_2O)_2]\cdot 2H_2O$, Displacement ellipsoids are drawn at the 50% probability level. (**b**) Coordination environment of Cu(II) complex.

angle of approximately 12.29° with the plane of pyrazine molecule (figure 3). In the crystal structure of **1**, extensive network of hydrogen bonds exists between dimers and uncoordinated water molecules (figure 4).

As is shown in figure 5, the carboxyl groups of $(pydc)^{2-}$ and water molecules are involved in intermolecular O−H···O hydrogen bonding and form three types of robust hydrogen bond networks, namely, R_2^2 (8) **I**, R_3^2 (15) **II** and R_5^6 (24) **III**. These intermolecular interactions connected the dimeric complexes and water molecules into a 3D-network. In addition, two types of weak C−H···O hydrogen bonds connected the neutral complexes to form 2D sheets. Another characteristic feature of this crystal structure is the presence of C−O···π interactions [O···centroid distances = 3.477(13) Å and 3.791(14) Å] occur between C1-O2 and Cg3 [Cg3 = N1/C2-C6] and C7-O4 and Cg3 (figure 5). The O–H···O hydrogen bonds occur both within a stack of dimers along the crystallographic a-axis and between dimers of different stacks. Within a stack of dimers along the a-axis, the O–H···O hydrogen bond is between a coordinated water oxygen atom in one dimer and an uncoordinated carboxylate oxygen atom in a neighboring dimer. This hydrogen bond (O5–H5A···O4) has a bond angle of 168° and a distance of 2.753(16) Å between the two oxygen atoms. Interestingly, extension this kind of hydrogen bond interactions makes fascinating 2D porosity sheets as shown in figure 6. The second type of O–H···O hydrogen bond occurs between uncoordinated water molecules and uncoordinated carboxylate oxygen atoms of $(pydc)^{2-}$ ligands and these water molecules are located in the cavities.

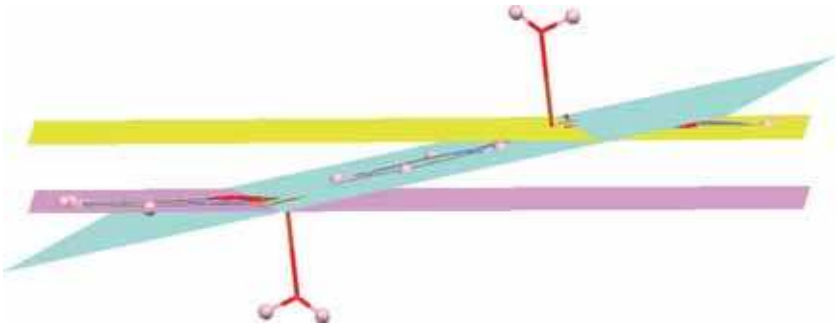

Figure 3. A view of different planes in Cu(II) complex.

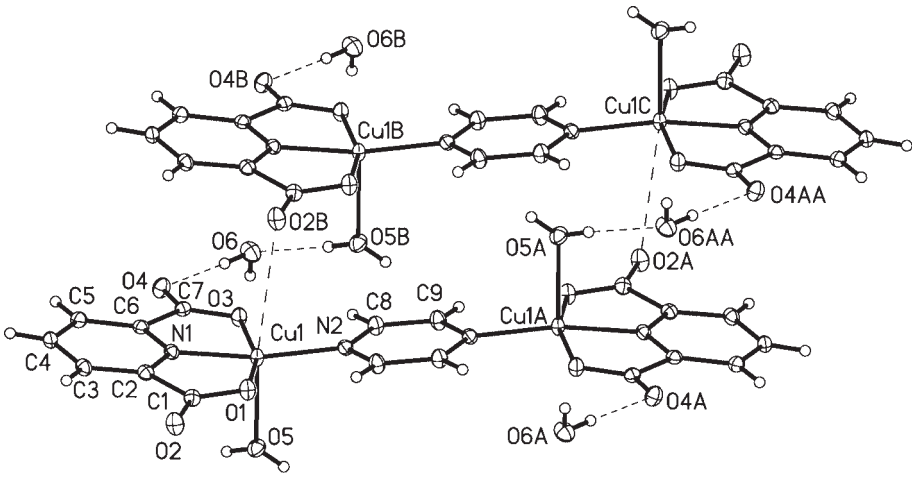

Figure 4. A view of hydrogen bond interactions in $[Cu_2(pydc)_2(pz)\ (H_2O)_2]\cdot 2H_2O$.

The D···A distance for this hydrogen bond (O6–H6B···O4) is 2.868(17) Å and its bond angle is 177°. The third O–H···O hydrogen bond which incorporated in forming the cavities takes place between O5–H5B···O6 with D···A distance about 2.726 (18) Å and 174°.

3.3 *Thermal analysis*

The thermal behavior of compound **1** was studied at room temperature to 1000°C in N_2 atmosphere. The endothermic peak of **1** between 40 and 200°C, correspond to loss of 4-moles of water molecules (found 11%

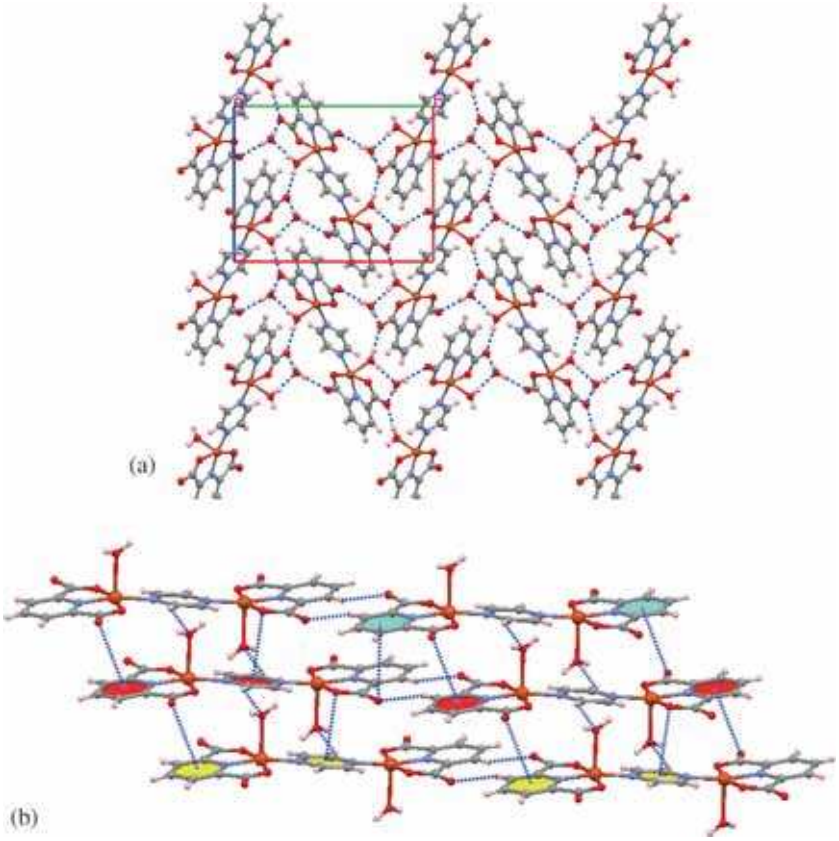

Figure 5. (**a**) The extended 2D network of compound **1** interconnected by O–H···O hydrogen bonds, uncoordinated water molecules and neighboring stacks of dimers. (**b**) A view showing how the dimeric complexes are connected by O–H···O, C–H···O and C–O···π interactions (blue dashed lines) to form 2D sheet.

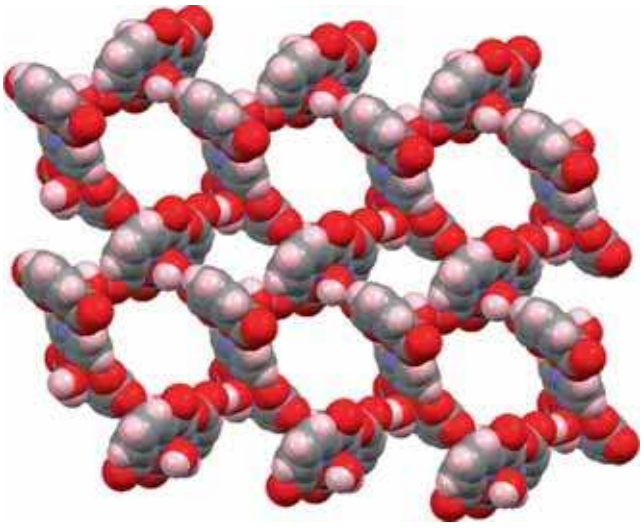

Figure 6. Porous network resulted from O–H···O type interaction in the crystal lattice of **1**.

and calc. 11.81%). The TG curve shows that the complex starts to decompose with the gradual release the organic moiety. The final decomposition product was CuO (found 15.20%, calc. 13.05%).

3.4 *Properties of the Cu-PDAP/CNTs/GC electrode*

Electrodeposition of Cu-PDAP at the surface of CNTs/GC electrode was carried out by immersion *CNTs/GC* electrode in 1.0×10^{-2} M Cu-PDAP in DMSO-acetate buffer solutions with 0.1 M tetrabuthyl ammonium perchlorate (figure 7a). The potential was continuously cycled between −400 and 700 mV at the potential sweep rate of 50 mV s^{-1}. In the first cycle, a well-defined irreversible anodic peak appears at a potential of about 20 mV that may be due to adsorption of Cu-PDAP and its oxidation product on the electrode surface (this anodic peak corresponding to PDAP oxidation) (figure 7b). This anodic peak disappeared in the next cycle and new anodic and cathodic peaks corresponding to Cu(II)-PDAP /Cu(I)-PDAP appeared around 310 and 110 mV, respectively. Consecutive cyclic voltammograms showed that the thickness of Cu-PDAP film grows through each cycle during the electrodeposition of Cu-PDAP complex (figure 7a). The anodic and cathodic peak currents did not alter upon further potential cycling (more than 50 cycles).

The results show that not only the peak currents increase steadily with increasing the scan number but also their anodic and cathodic peaks potential shifted towards positive and negative values, respectively. These results confirm the continuous deposition of Cu-PDAP film at the electrode surface. The same results have been previously reported.[39,40] The redox reaction that occurs during cycles is related to the Cu(I)-PDAP/ Cu(II)-PDAP transition.[41] As can be seen in figure 7a, the formal potential ($E^{0'}$) is about 0.21 V versus the reference electrode and the difference between anodic and cathodic peak potential is about 96 mV.

To investigate the effect of PDAP on modification of the electrode, modified electrode was made from 0.1 M tetrabuthyl ammonium perchlorate containing $CuCl_2$ (a) and Cu-PDAP (b) and the resulting electrodes were denoted as a Cu/CNTs/GC and Cu-PDAP/CNTs/GC, respectively (figure 8). As it is seen, a pair of ill-defined redox peaks were observed when Cu/CNTs/GC electrode was used (curve a). On the other hand, a pair of well-defined redox peaks were observed when Cu-PDAP/CNTs/GC electrode was used (curve b). So, there is a considerable enhancement in the charge of voltammogram in the presence of PDAP (about ten times).

It is well known that in aqueous media the oxidation of metal ions is very difficult that may be due

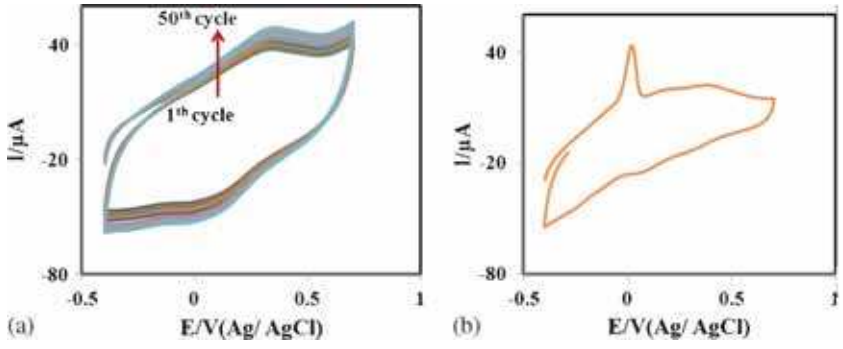

Figure 7. (**a**) Consecutive cyclic voltammograms of CNTs/GC electrode in 1.0×10^{-2} M Cu-PDAP in DMSO-acetate buffer solution with 0.1 M tetrabuthyl ammonium perchlorate at a scan rate of 50 mVs^{-1} (every five cycles). (**b**) First cycle of CNTs/GC electrode in the same solution.

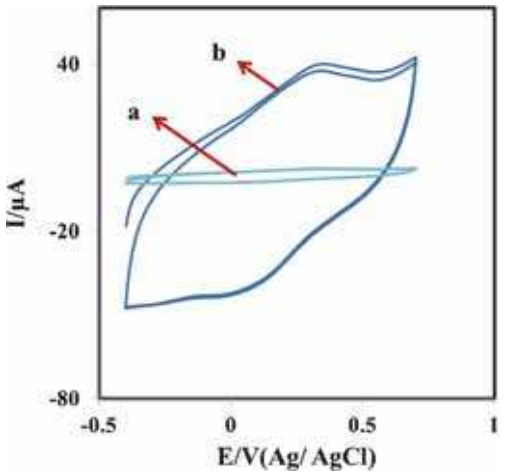

Figure 8. Cyclic voltammograms of Cu/CNTs/GC electrode (curve a), and Cu-PDAP/ CNTs/GC electrode (curve b), in 0.25 M acetate buffer solution at a scan rate of 50 mVs^{-1}.

to the strong hydration of ions.[42] Therefore, when copper ion is coordinated by PDAP, its oxidation conditions can be changed significantly and the Cu(I)-PDAP/Cu(II)-PDAP redox couple is observed in the Cu-PDAP film.

3.5 *Electrocatalytic oxidation of L-cysteine at Cu-PDAP/CNTs/GC electrode*

Application of the modified electrode for oxidation *L-cysteine* was evaluated by cyclic voltammetry. The cyclic voltammetric responses of GC, CNTs/GC, Cu-PDAP/GC and Cu-PDAP/CNTs/GC electrodes in 0.25 M acetate buffer solution without and with L-cysteine in solution were studied (figure S2). The results show that, L-cysteine did not undergo oxidation at GC and CNTs/GC electrodes in the potential range of −0.5–0.6 V (curves b and d). When GC electrode was modified with Cu-PDAP film (Cu-PDAP/GC) and then inserted into the same L-cysteine-containing electrochemical cell, a small electrocatalytic activity was observed for L-cysteine oxidation (curve f). Modification of the GC electrode with multiwall carbon nanotube improved the electroactivity of Cu-PDAP/CNTs/GC electrode for oxidation of L-cysteine (curve h). When Cu-PDAP film deposited on multiwall carbon nanotube was used as a modified electrode in the same solution a large anodic current was observed with a small cathodic counterpart. The observed current is associated with L-cysteine oxidation. Whereas L-cysteine was not oxidized at the surface of GC and CNT/GC electrodes, electroactivity toward L-cysteine on modified electrode (Cu-PDAP/CNTs/GC) was significant.

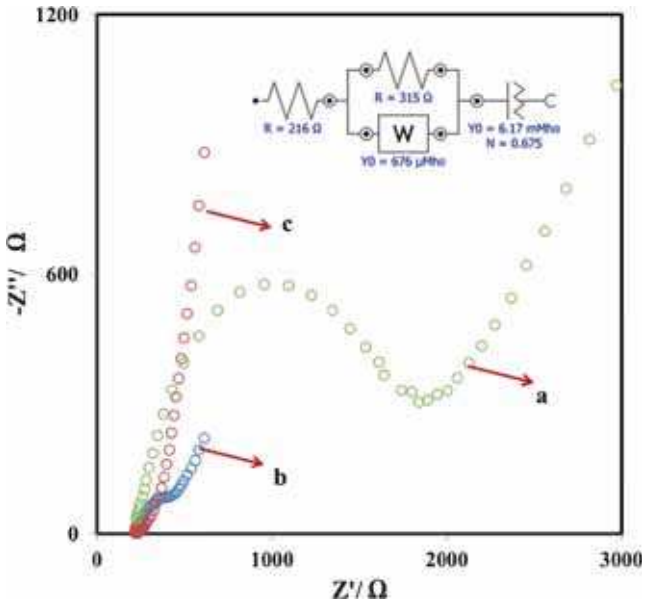

Figure 9. Nyquist plots of bare GC electrode (curve a), Cu-PDAP/GC (curve b), and Cu- PDAP/CNTs/GC (curve c) in 0.1 M KCl solution containing 5 mM of L-cysteine. Inset: Equivalent circuit used to model impedance data in the presence of redox couples. Conditions: potential = 0.35 V, frequency range of 10 kHz–0.1 Hz, A= 0.0534 cm^2 and pH=6.

Upon addition of L-cysteine, an enhancement in the anodic peak current was observed and the cathodic peak current tended to decrease. The reason for this increase is that, along with the anodic potential sweep, L-cysteine reduces Cu(II)-PDAP to Cu(I)-PDAP, while simultaneous oxidation of the regenerated Cu(I)-PDAP causes an increase in the anodic current. For the same reason, the cathodic current is smaller in the presence of L-cysteine, indicating that Cu(II)-PDAP is consumed during a chemical step.

Taking into account all these observations, a possible mechanism of L-cysteine electrooxidation on Cu-PDAP/CNTs/GC electrode may be as follows:

$$\left[\mathrm{Cu^{II}\text{-}PDAP}\right]^{+} + \mathrm{e^{-}} \longrightarrow \left[\mathrm{Cu^{I}\text{-}PDAP}\right] \qquad (1)$$

$$2\left[\mathrm{Cu^{II}\text{-}PDAP}\right]^{+} + 2\mathrm{CySH} \rightarrow 2\left[\mathrm{Cu^{I}\text{-}PDAP}\right] + \mathrm{CyS\text{-}SCy} + 2\mathrm{H^{+}} \qquad (2)$$

Such a behavior is indicative of an EC′ mechanism. On the other hand, the increased current in the oxidation region is due to the fact that the L-cysteine present in solution diffuses toward the electrode and reduces Cu(II)-PDAP which is produced electrochemically. As Cu (I)-PDAP is regenerated by L-cysteine during the potential sweep, there is a resultant increase in the anodic current.

Electrochemical impedance spectroscopy (EIS) technique has been proved as an effective method for

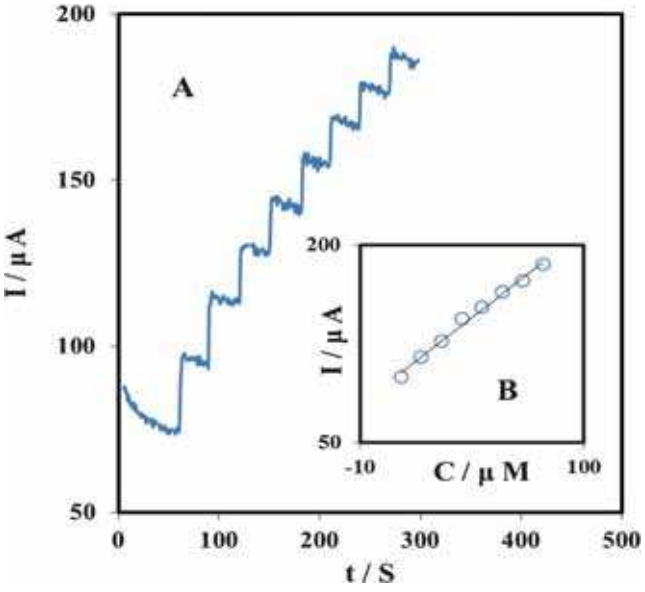

Figure 10. (A) Amperometric response of rotating sensor for successive addition of 10 μM L-cysteine; conditions: potential = 0.35 V and rotating speed of 2000 rpm. (B) Plot of amperometric current vs. L-cysteine concentration.

probing the features of surface modified electrodes. To understand the electrochemical reactions at the different modified electrodes, the EIS experiments were performed in the presence of 5 mM of L-cysteine. Figure 9 shows the typical Nyquest plots for bare GC, Cu-PDAP/GC, and Cu-PDAP/CNTs/GC in 0.1 M KCl solution containing 5 mM of L-cysteine as an electrochemical redox marker. The straight line at low frequency is related to the diffusion process known as Warburg element, while the high frequency semicircle is related to the electron transfer resistance (R_{et}), which controls the electron transfer kinetics of the redox probe at the electrode interface.

As can be seen in figure 9 for GC electrode, a semicircle is observed over the whole frequency region and the value of R_{ct} is 315 Ω, indicating that the reaction is kinetically controlled (figure 9a). After immobilization of Cu-PDAP at the surface of GC electrode, the value of R_{ct} is significantly decreased to about 54 Ω (figure 9b). The results indicate that the immobilized Cu-PDAP decreases the charge transfer kinetics to about one-sixth of that at the bare GC electrode and it also confirmed that the presence of Cu-PDAP film on GC electrode had a catalytic effect for oxidation of L-cysteine. For Cu-PDAP/CNTs/GC (figure 9c) electrode the calculated charge transfer resistance is less, which proves that the assembly of CNTs make the electron transfer easier. The deposition of CNTs on the surface of modified electrode facilitated the electron transfer of the electrochemical probe on the modified electrode.

3.6 *Amperometric detection of L-cysteine at the modified electrode*

Since amperometry under stirred conditions is more sensitive than cyclic voltammetry, it was used to estimate the lower limit of detection. Figure 10A displays a typical steady-state catalytic current-time response of the rotated modified electrode (2000 rpm) with successive injection of 10 μM L-cysteine, at a fixed potential of 0.35 V vs. reference electrode. As shown, during successive addition of L-cysteine, a well-defined response was observed, demonstrating stable and efficient catalytic ability of the Cu-PDAP immobilized on the multiwall carbon nanotube glassy carbon electrode.

The response current is linear in the range of 10–80 μM of L-cysteine (figure 10B). The calibration plot has a correlation coefficient of 0.998 and the detection limit of 2.1 μM at signal to noise ratio of 3. Detection limit and linear calibration range of the proposed modified electrode were compared with those previously reported, and the results are summarized in table 4. As can be seen, the analytical parameters are comparable or better than the results reported for L-cysteine determination at the surface of other modified electrodes (table 4).

4. Conclusion

A Cu(II) dimer complex $[Cu_2(pydc)_2(pz)(H_2O)_2].2H_2O$ has been synthesized and characterized. Neighboring dimers are connected to each other through extensive hydrogen bonding network. The layers of

Table 4. Electrochemical response for L-cysteine using various modified electrodes

Electrode	Analyte	LOD (μM)	Linear range (μM)
MWCNTs-modified GCE[43]	CySH	5.4	10.0–500
PolyN,Ndimethylaniline/ferrocyanide film/CPE[44]	CySH	6.38	7.40–138
Ordered mesoporous carbon[45]	CySH	0.10	3.00–130
Copper-cobalt hexacyanoferrate/CPE[46]	CySH	5.00	6.00–1000
Cu-PDAP/CNTs/GC	CySH	2.10	10.0–80.0

complex are connected into a 3D supramolecular network by non-classical hydrogen bonds and C−H···O stacking interactions. Also, the porosity of the crystal structure was formed by these kinds of intermolecular interactions. Oxidation of cysteine on the surface of modified electrode based on Cu(II) complex was investigated with cyclic voltammetry and electrochemical impedance spectroscopy (EIS) and the results showed that the Cu-PDAP/CNTs film displays excellent electrochemical catalytic activity towards L-cysteine oxidation.

Supplementary Information

CCDC 1402561 contains the supplementary crystallographic data for **1**. These data can be obtained free of charge at http://www.ccdc.cam.ac.uk/conts/retrieving.html, or from the Cambridge Crystallographic Data Center, 12 Union Road, Cambridge CB2 1EZ, UK (fax: 0044 1223 336 033; e-mail: deposit@ccdc.cam.ac.uk). Supplementary Information is available at www.ias.ac.in/chemsci.

References

1. Yaghi O M, OKeeffe M, Ocking N W, Chae H K, Eddaoudi M and Kim J 2003 *Nature* **423** 705
2. Moulton B and Zaworotko M J 2001 *Chem. Rev.* **101** 1629
3. Biradha K, Su C Y and Vittal J 2011 *Cryst. Growth Des.* **11** 875
4. Demessence A and Long J R 2010 *Chem. Eur. J.* **16** 5902
5. Abrahams B F, Grannas M J, Hudson T A and Robson R 2010 *Angew. Chem. Int. Ed.* **49** 1087
6. Ke X J, Li D S and Du M 2011 *Inorg. Chem. Commun.* **14** 788
7. Rao C N R and Natarajan S 2004 *Angew. Chem. Int. Ed.* **43** 1466
8. Allendof M D, Bauer C A, Bhakta R K and Houk R J T 2009 *Chem. Soc. Rev.* **38** 1330
9. Lee J Y, Farha O K, Roberts J, Scheidt K A, Nguyen S T and Hupp J T 2009 *Chem. Soc. Rev.* **38** 1450
10. Murray L J, Dinca M and Long J R 2009 *Chem. Soc. Rev.* **38** 1294
11. Kurmoo M 2009 *Chem. Soc. Rev.* **38** 1353
12. Forster P M, Stock N and Cheetham A K 2005 *Angew. Chem. Int. Ed.* **44** 7608
13. Zhou Y F, Lou B Y, Yuan D Q, Xu Y Q, Jiang F L and Hong M H 2005 *Inorg. Chim. Acta* **358** 3057
14. Chen S M, Lu C Z, Zhang Q Z, Liu J H and Wu X Y 2005 *Eur. J. Inorg. Chem.* **2** 423
15. Biswas R, Mukherjee S, Ghosh S, Diaz C and Ghosh A 2015 *Inorg. Chem. Commun.* **56** 108
16. Mahmudov K T, Haukka M, Sutradhar M, Mizar A, Kopylovich M N and Pombeiro A J L 2013 *J. Mol. Struct.* **1033** 127
17. Watanabe R, Shimada T, Koyama N, Ishida T and Kogane T 2011 *Polyhedron* **30** 3165
18. Wriedt M and Zhou H C 2012 *Dalton Trans.* **41** 4207
19. Ene C D, Lungu A, Mihailciuc C, Hillebrand M, C R P and M Andruh 2012 *Polyhedron* **31** 539; (b) Zhang T, Wang D F, Huang R B and Zheng L S 2015 *Inorg. Chim. Acta* **427** 299
20. Thomas R and Kulkarni G U 2008 *J. Mol. Struct.* **873** 160
21. Perpétuo G J and Janczak J 2008 *J. Mol. Struct.* **891** 429
22. Lu B Y, Li H, Deng H, Xu Z H, Li W S and Chen H Y 2008 *J. Electroanal. Chem.* **621** 97
23. Li J, Yu Q and Peng T 2005 *Anal. Sci.* **21** 377
24. Sun X, Li R, Villers D, Dodelet J P and Desilet S 2003 *Chem. Phys. Lett.* **379** 99
25. Dai X, Wildgoose G G and Compton R G 2006 *Analyst* **131** 901
26. Ozoemena K I, Nyokong T, Nkosi D, Chambrier I and Cook M J 2007 *Electrochim. Acta* **52** 4132
27. *Programs Apex 2 and SAINT* 2009 (Madison, Wisconsin, USA: Bruker AXS Inc.)
28. Sheldrick G M 2008 *Acta Crystallogr.* **A64** 112
29. Derikvand Z, Bruno G, Amiri Rudbari H, Shokrollahi A, Zarghampour F and Azadbakht A 2014 *Inorg. Chim. Acta* **410** 221
30. Kirillova M V, Da Silva M F C G, Kirillov A M, Da Silva J J R F and Pombeiro A J L 2007 *Inorg. Chim. Acta* **360** 506
31. Vargova Z, Zeleoak V, Cisaova I and Györyova K 2004 *Thermochim. Acta* **423** 149
32. Mao L, Wang Y, Qi Y, Cao M and Hu C 2004 *J. Mol. Struct.* **688** 197
33. Uçar I, Karabulut B, Bulut A and Büyükgüngör O 2007 *J. Mol. Struct.* **834–836** 336
34. Cotton FA 1980 In *Advanced Inorganic Chemistry* (New York: Wiley-Interscience) p. 642
35. Derikvand Z, Talei G R, Aghabozorg H, Olmstead M M, Azadbakht A, Nemati A and Attar Gharamaleki J 2010 *Chin. J. Chem.* **28** 2167
36. Kroczewska D, Kurzak B and Jezierska J 2006 *Polyhedron* **25** 678
37. Ghosh M, Majee A, Nethaji M and Chattopadhyay T 2009 *Inorg. Chim. Acta* **362** 2052
38. Tabatabaee M, Bordbar M, Ghassemzadeh M, Tahriri M, Tahrir M, Mehri L Z and Neumüller B 2013 *Eur. J. Med. Chem.* **70** 364
39. Ciszewski A, Milczarek G, Lewandowska B and Krutowski K 2003 *Electroanalysis* **15** 518
40. Vilas-Boas M, Freire C, Castro B and Hillman A R 1998 *J. Phys. Chem. B* **102** 8533
41. Salimi A, Korani A, Hallaj R, Khoshnavazi R and Hadadzadeh H 2009 *Anal. Chim. Acta* **635** 63
42. Ciszewski A 1995 *Electroanalysis* **7** 1132
43. Salimi A and Hallaj R 2005 *Talanta* **66** 967
44. Ojani R, Raoof J B and Zarei E 2010 *J. Electroanal. Chem.* **638** 241
45. Ndamanisha J C, Bai J, Qi B and Guo L 2009 *Anal. Biochem.* **386** 79
46. Abbaspour A and Ghaffarinejad A 2008 *Electrochim. Acta* **53** 6643